Supplementary Information

Europium(II) Complexes with Substituted Triethylenetetramine: New Emitters to Construct Efficient Deep Blue Organic Light Emitting Diodes by Spin Coating

Hao Qi, Tianming Zhong, Peihao Huo, Jiayin Zheng, Zifeng Zhao, Wenchao Yan, Zuqiang Bian,* and Zhiwei Liu*

Beijing National Laboratory for Molecular Sciences (BNLMS), State Key Laboratory of Rare Earth Materials Chemistry and Applications, Beijing Engineering Technology Research Centre of Active Display, College of Chemistry and Molecular Engineering, Peking University, Beijing, 100871, China

Emails: bianzq@pku.edu.cn, zwliu@pku.edu.cn

I. General details

General methods: ^{1}H NMR spectra were recorded on Bruker 400MHz NMR spectrometer. Electrospray ionization mass spectra (ESI-MS) were performed in positive ion mode on Bruker Apex IV Fourier transform ion cyclotron resonance mass spectrometer. Elemental analyses were conducted on a VARIO elemental analyzer from Elementar Analysensysteme GmbH.

Photophysical Measurements: Ultraviolet-visible (UV-vis) absorption spectra were measured by a Shimadzu UV-3600Plus UV-VIS-NIR spectrometer. Excitation and emission spectra were recorded on Edinburgh FLS980 fluorescence spectrophotometer. Luminescence lifetimes were obtained on a single photon counting spectrometer from Edinburgh FLS980 with laser lamp as the excitation source. The data were analyzed by tail fit of the decay profile using a software package provided by Edinburgh Instruments. Absolute photoluminescence quantum yields (PLQYs) were measured using Hamamatsu C9920-02 PLQY measurement system with integrating sphere for all the complexes. All measurements were performed at room temperature

Single Crystal Structure Measurements: The single crystal X-ray diffraction (SCXRD) data were collected on a Rigaku Mercury CCD diffractometer. The radiation used in the SCXRD analysis is the graphite-mon chromated Mo Kα emission line (λ= 0.71069 Å). SCXRD data were collected by using the CrystalClear software. Structural refinements were conducted with SHELXL-97 or SHELXL-2013 software. The X-ray crystallographic coordinates for the structures reported in this article have been deposited at the Cambridge Crystallographic Data Centre (CCDC). These data can be obtained free of charge from the CCDC via www.ccdc.cam.ac.uk/data_requ est/cif.

Cyclic Voltammetry Measurement: Cyclic voltammetry was carried out in degassed DCM solution (10^{-3} M) at room temperature with a CHI600C voltametric analyzer. Tetrabutylammonium hexafluorophosphate ($TBAPF_6$, 0.1 M) was used as the supporting electrolyte. The conventional three-electrode configuration includes a

platinum working electrode, a platinum wire auxiliary electrode, and an Ag/AgCl wire pseudo-reference electrode. The scan rate is 100 mV s^{-1}.

OLEDs Fabrication and Measurement: In the process of solvent screening, we took $N_4Me_2Et_4$-EuI_2 as a representative and tried a variety of common solvents, such as toluene, methanol, acetonitrile, dichloromethane, and their binary mixtures. Among them, toluene is hard to dissolve the complex, while the spin coated films from methanol, acetonitrile and dichloromethane solutions are uneven (visible to the naked eye). So, we took it a step further by dissolving $N_4Me_2Et_4$-EuI_2 in a mixed solvent. It is found that the films obtained from methanol/toluene (1:1) and acetonitrile/toluene (1:1) are smooth. However, the two films showed PLQY of 3% and 35%, respectively. Hence, we optimized the ratio of acetonitrile and toluene, since more acetonitrile results in better solubility while worse uniform and lower PLQY of the film. Finally, we selected an acetonitrile/toluene mixture with a volume ratio of 1:3 as the solvent to prepare devices. Indium tin oxide (ITO) patterned anode was commercially available with a sheet resistance of 14 Ω $square^{-1}$ and 80 nm thickness. ITO substrates were cleaned with deionized water and ethanol[1]. Then, the ITO-coated glass was treated with oxygen plasma for 10 min, spin-coated with poly(3,4-ethylenedioxythiophene): polystyrene sulfonate (PEDOT: PSS, Clevios P VP AI 4083) at 500 rpm for 9 s and 4000 rpm for 60 s. Then, the PEDOT: PSS-coated ITO glass was transferred to a glove box and annealed at 120 °C for 20 min. Poly(N-vinylcarbazole) (PVK, Approx. Mw 90000, Shanghai Aladdin Biochemical Technology Co., Ltd) were dissolved in toluene then spin-coated at 4000 rpm for 30 s. The samples were annealed at 130 °C for 20 min to remove the residual solvent. Then N_4Me_6-EuI_2, $N_4Me_2Et_4$-EuI_2 and $N_4Me_2Pr_4$-EuI_2 was dissolved in mixed solvent (toluene:acetonitrile = 3:1), and 9,9-dimethyl-10-(9-phenylcarbazol-3-yl)acridine (PCzAc) were dissolved in toluene. The two solutions were mixed with different weight ratios. The blended emission layers (EMLs) were spin-coated at 3000 rpm for 30 s. The electron transport layer and metal layer were deposited in different vacuum chambers with a base pressure better than 1×10^{-4} Pa. The active area for each device is 4 mm^2. PCzAc and oCBP were synthesized according to

the previous reports[2, 3]. The compounds were purified by gradient thermal sublimation and their purities were characterized by ^{1}H NMR. mCP was commercially available from Jilin OLED Materials Tech Co., Ltd. Its purity is 99.5%. The chemical structures of PCzAc, mCP and oCBP are shown in **Figure S8**. All electric testing and optical measurements were performed under ambient conditions. The electroluminescence spectra, current density-voltage-luminance (J-V-L) curves, current efficiency–luminance–external quantum efficiency (CE-L-EQE) curves and EQEs characteristics were measured by computer controlled Keithley 2400 source meter and absolute EQE measurement system (C9920-12) with photonic multichannel analyzer (PMA-12, Hamamatsu Photonics). Atomic force microscope (AFM) was performed using an ICON2-SYS (Bruker Nano) microscope.

II. Supplementary Figures and Tables

Table S1. Crystallographic data for N_4Me_6-EuI_2, $N_4Me_2Et_4$-EuI_2 and $N_4Me_2Pr_4$-EuI_2.

Compound	N_4Me_6-EuI_2	$N_4Me_2Et_4$-EuI_2	$N_4Me_2Pr_4$-EuI_2
chemical formula	$C_{16}H_{36}EuI_2N_4$	$C_{20}H_{44}EuI_2N_4$	$C_{44}H_{92}Eu_2I_4N_4O_5$
formula weight	690.25	746.35	1568.73
crystal size (mm)	0.08×0.03×0.02	0.08×0.04×0.02	0.05×0.04×0.02
temperature (K)	180(10)	180(10)	180(10)
radiation	0.71073	0.71073	0.71073
crystal system	monoclinic	monoclinic	monoclinic
space group	P 21/c	C 2	C 2
a(Å)	16.0897(3)	13.2806(3)	13.4959(2)
b(Å)	8.7529(2)	11.8453(3)	11.8913(2)
c(Å)	17.4038(4)	8.9150(2)	18.6407(3)
α(°)	90	90	90
β(°)	105.998(2)	108.362(3)	98.846(2)
γ(°)	90	90	90
V(Å^3)	2356.08(9)	1331.04(6)	2955.95(8)
Z	4	2	2
$\rho_{(calc)}$ (g/cm^3)	1.946	1.862	1.763
F (000)	1316	722	1524
absorp. coeff. (mm^{-1})	5.288	4.687	4.230
θ range (deg)	2.428-30.773	2.359-29.446	2.221-30.641
reflns collected	56968 (R_{int} = 0.0443)	8378 (R_{int} = 0.0320)	36315 (R_{int} = 0.0448)
indep. reflns	6711	3009	8080
refns obs. [$I>2\sigma(I)$]	5323	2924	6847
data/restr/paras	6711/0/214	3009/46/138	8080/86/307
GOF	1.014	1.051	1.012
R_1/wR_2 [$I>2\sigma(I)$]	0.0298/0.0659	0.0264/0.0649	0.0324/0.0675
R_1/wR_2 (all data)	0.0447/0.0709	0.0276/0.0655	0.0415/0.0696

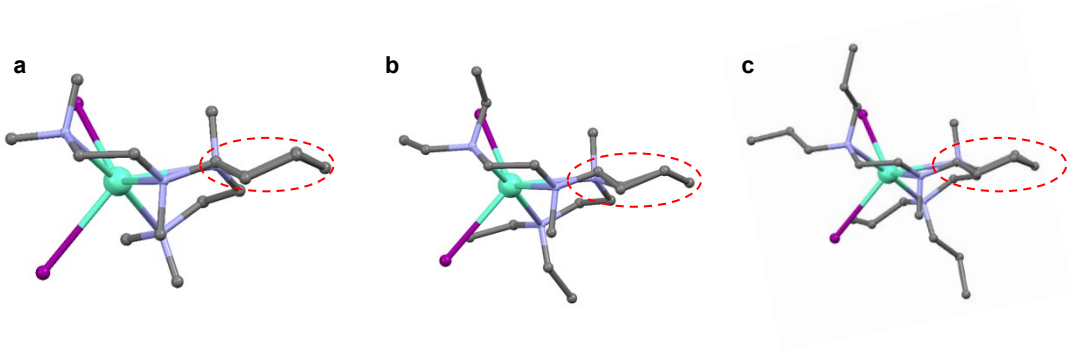

Figure S1. The chair conformation of cyclohexane groups in (a) N_4Me_6-EuI_2, (b) $N_4Me_2Et_4$-EuI_2 and (c) $N_4Me_2Pr_4$-EuI_2.

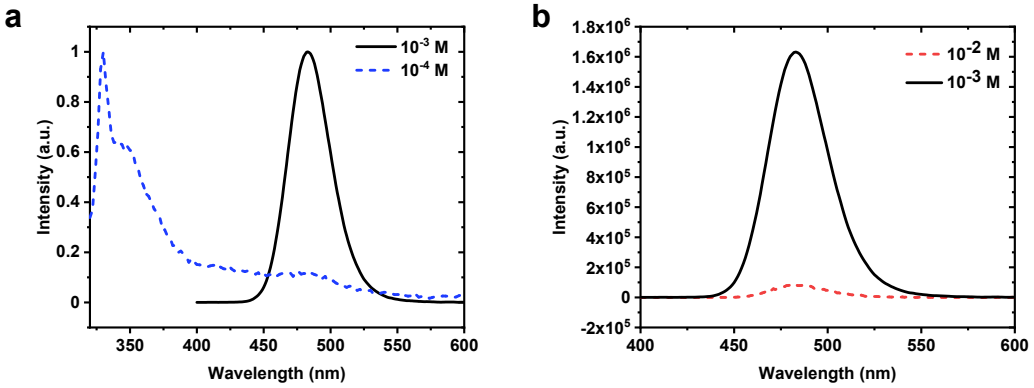

Figure S2. (a) The normalized emission spectra of N_4Me_6-EuI_2 in DCM solutions at concentrations of 10^{-3} M and 10^{-4} M. (b) The emission spectra of N_4Me_6-EuI_2 in DCM solutions at concentrations of 10^{-2} M and 10^{-3} M with same slit width.

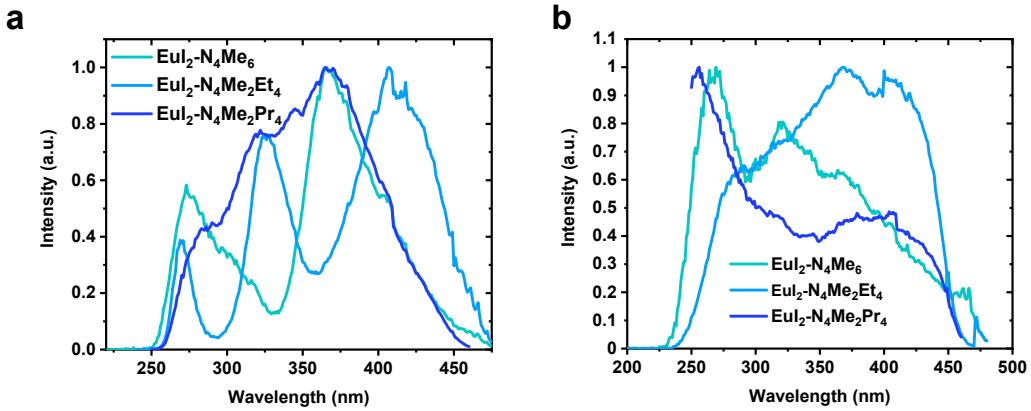

Figure S3. Excitation spectra of N_4Me_6-EuI_2, $N_4Me_2Et_4$-EuI_2 and $N_4Me_2Pr_4$-EuI_2 in DCM (10^{-3} M) (a) and crystalline powder (b). The detected wavelength is determined by the peak emission of each complex, i.e. 478, 466, 466 nm in solution and 481, 465, and 465 nm in crystalline powder for N_4Me_6-EuI_2, $N_4Me_2Et_4$-EuI_2 and $N_4Me_2Pr_4$-EuI_2, respectively.

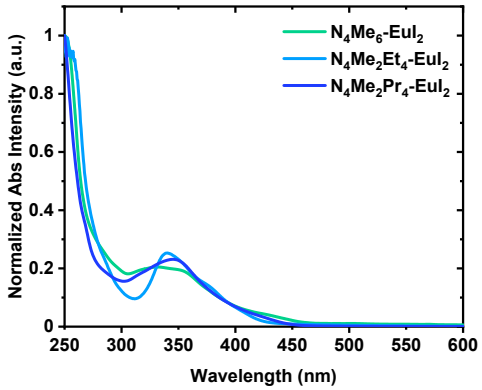

Figure S4. UV-vis spectra of N_4Me_6-EuI_2, $N_4Me_2Et_4$-EuI_2 and $N_4Me_2Pr_4$-EuI_2 in DCM (10^{-3} M).

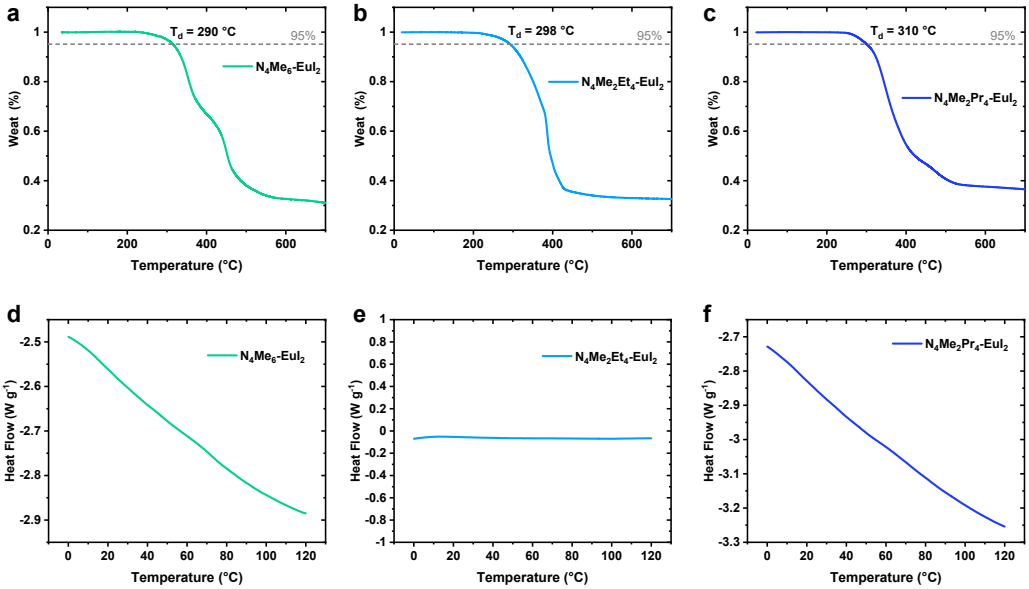

Figure S5. TGA curves of N_4Me_6-EuI_2 (a), $N_4Me_2Et_4$-EuI_2 (b) and $N_4Me_2Pr_4$-EuI_2 (c). T_d represents the decomposition temperature at 5% weight loss. DSC curves of N_4Me_6-EuI_2 (d), $N_4Me_2Et_4$-EuI_2 (e) and $N_4Me_2Pr_4$-EuI_2 (f).

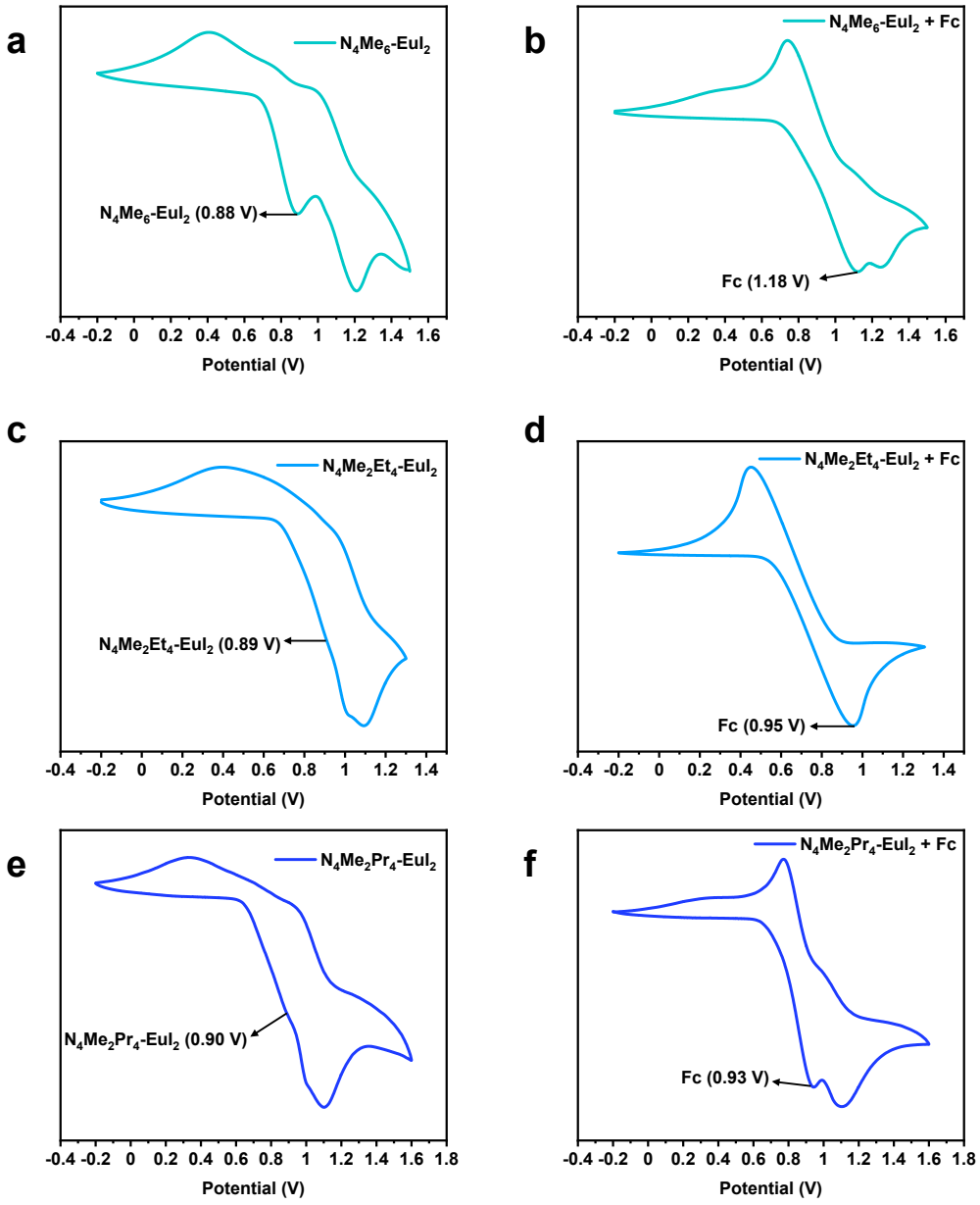

Figure S6. The cyclic voltammograms of (a) N_4Me_6-EuI_2, (b) N_4Me_6-EuI_2+ Fc, (c) $N_4Me_2Et_4$-EuI_2, (d) $N_4Me_2Et_4$-EuI_2 + Fc, (e) $N_4Me_2Pr_4$-EuI_2 and (f) $N_4Me_2Pr_4$-EuI_2 + Fc in DCM (10^{-3} M).

Table S2 The deduced energy levels of the Eu(II) complexes.

	HOMO (eV)	Absorption edge (nm)	E_g(eV)	LUMO (eV)
N_4Me_6-EuI_2	-4.3	463	2.7	-1.6
$N_4Me_2Et_4$-EuI_2	-4.5	456	2.7	-1.8
$N_4Me_2Pr_4$-EuI_2	-4.5	450	2.8	-1.8

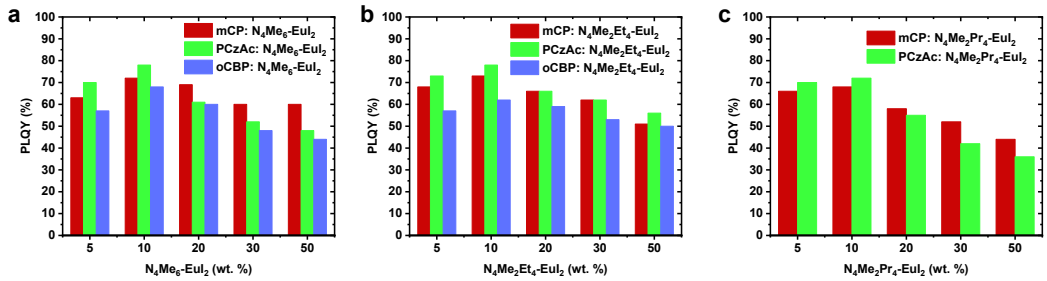

Figure S7. The PLQYs of Eu(II) complexes in different host materials with different doping concentrations. (a) The PLQYs of N_4Me_6-EuI_2 doped in mCP, PCzAc and oCBP with different doping concentrations, (b) The PLQYs of $N_4Me_2Et_4$-EuI_2 doped in mCP, PCzAc and oCBP with different doping concentrations, (c) The PLQYs of $N_4Me_2Pr_4$-EuI_2 doped in mCP and PCzAc with different doping concentrations.

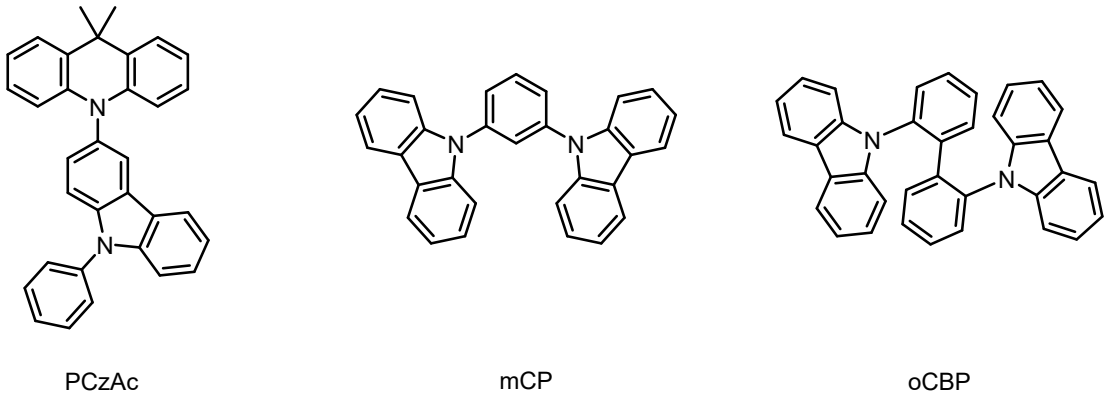

Figure S8. The chemical structures of PCzAc, mCP and oCBP.

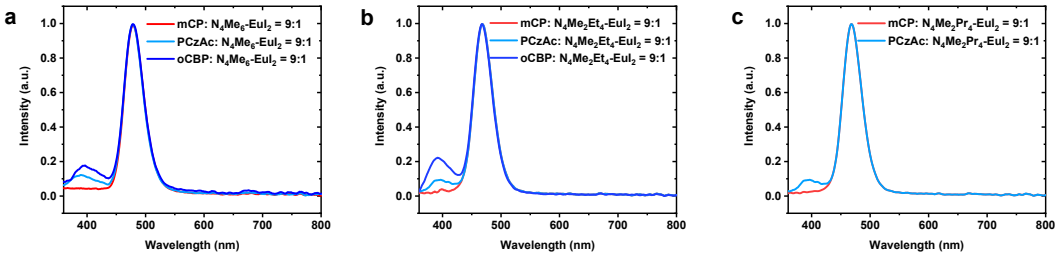

Figure S9. The photoluminescence spectra of some specific doped films with high PLQYs. (a) The photoluminescence spectra of N_4Me_6-EuI_2 doped in mCP, PCzAc and oCBP, (b) The photoluminescence spectra of $N_4Me_2Et_4$-EuI_2 doped in mCP, PCzAc and oCBP, (c) The photoluminescence spectra of $N_4Me_2Pr_4$-EuI_2 doped in mCP, and PCzAc.

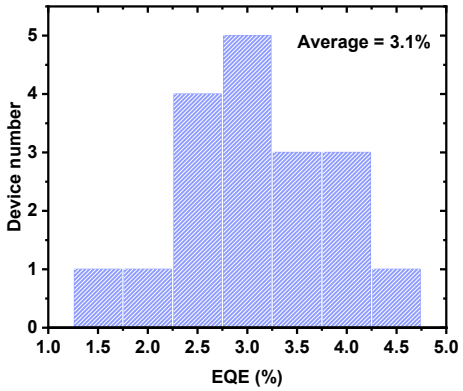

Figure S10. Maximum EQE histogram of 18 devices with the same device structure to the device of $N_4Me_2Et_4$-EuI_2 (average, ~3.1%; highest, 4.7%).

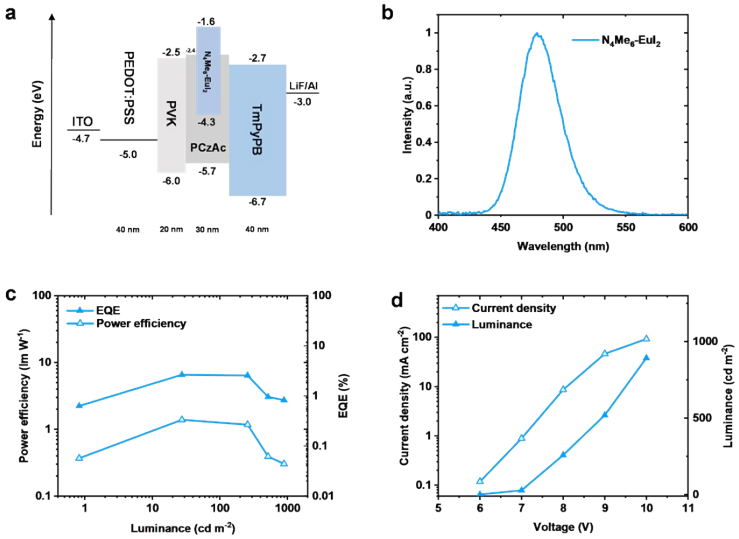

Figure S11. The performance of the device with N_4Me_6-EuI_2. (a) The optimized OLEDs structure with frontier orbital energy levels in electron volt of all organic materials and corresponding thickness. (b) Electroluminescence spectrum of the champion device at 7.0 V. (c) Power efficiency–luminance–external quantum efficiency (PE–L–EQE) curves of the champion device. (d) Current density–voltage–luminance (J–V–L) curves of the champion device.

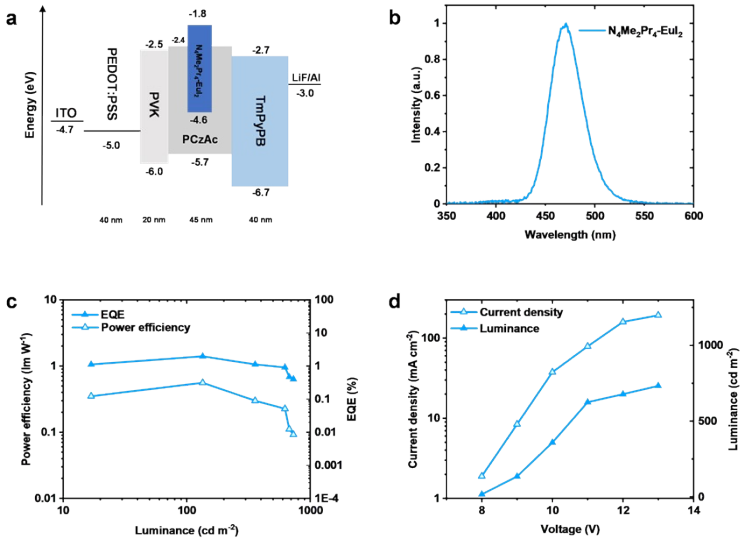

Figure S12. The performance of the device with $N_4Me_2Pr_4$-EuI_2. (a) The optimized OLEDs structure with frontier orbital energy levels in electron volt of all organic materials and corresponding thickness. (b) Electroluminescence spectrum of the champion device at 9.0 V. (c) Power efficiency–luminance–external quantum efficiency (PE–L–EQE) curves of the champion device. (d) Current density–voltage–luminance (J–V–L) curves of the champion device.

Reference:

1. J. Li, L. Wang, Z. Zhao, B. Sun, G. Zhan, H. Liu, Z. Bian and Z. Liu, *Nat Commun*, 2020, **11**, 5218.
2. V. Adamovich, J. Brooks, A. Tamayo, A. M. Alexander, P. I. Djurovich, B. W. D'Andrade, C. Adachi, S. R. Forrest, M. E. Thompson, *New J. Chem.* 2002, **26**, 1171.
3. S. Gong, X. He, Y. Chen, Z. Jiang, C. Zhong, D. Ma, J. Qin, C. Yang, *J. Mater. Chem.* 2012, **22**, 2894.